

Graph Denoising for Molecular Imaging

Master Thesis

Natural Science Faculty of the University of Basel
Department of Mathematics and Computer Science
Data-Analytics

Examiner: Prof. Dr. Ivan Dokmanić
Supervisor: Dr. Valentin Debarnot

Cédric Mendelin
cedric.mendelin@stud.unibas.ch
2014-469-274

12.06.2022

Acknowledgments

TODO

Abstract

TODO 100-250 words,

Table of Contents

Acknowledgments	ii
Abstract	iii
1 Introduction	1
2 Molecular Imaging methods	2
2.1 Computed tomography	2
2.2 Cryo-EM	4
2.3 Abstract form	7
3 Graph Denoising	9
3.1 Graph Foundations	9
3.1.1 Graph definition	9
3.1.2 Graph construction	10
3.2 Graph Denoising definition	11
3.2.1 Non-local means:	12
3.3 Graph Deep Learning	12
3.4 Graph Laplacian & Manifolds	13
3.4.1 Graph Laplacian	13
3.4.2 Manifolds	13
3.4.3 Manifold assumption	14
3.4.4 GL-manifold calculation	14
3.4.5 Manifold of computed tomography and cryo-EM	14
4 GAT-Denoiser	18
4.1 Concept	18
4.2 Components	19
4.2.1 Graph Attention Networks	20
4.2.2 Convolution	21
4.2.3 U-Net	21
4.3 Architecture	22
4.3.1 Layers	22
4.3.2 Training	23

5	Results	24
5.1	Dataset	24
5.2	Training setup	24
5.3	Source code	24
5.3.1	Python packages	25
5.4	Small Experiments	25
5.5	Complete Experiments	25
	Bibliography	26
	Appendix A Mathematical tools	28
A.1	signal-to-noise-ratio (SNR)	28
A.2	3D rotation matrix	28
A.3	Power Iterations	28

1

Introduction

Inverse problems aim to estimate an original signal that went through a system, based on (noisy) output signal observations. Machine learning (ML) is a tool to model and solve such inverse problems. They are widely used throughout different science directions, such as ML, signal processing, computer vision, natural language processing and others.

In recent years, graphs got a lot of attention in ML and are one of the most promising research areas. Graphs are a well suited data structure, simple but with high expressiveness. For some scenarios, ordinary ML algorithm fail, but Graph ML approaches have great success, e.g. dimensionality reduction for high-dimensional data. Data can be in a graph structure already, like social networks, or they can be constructed for arbitrary datasets.

Cryo-electron microscopy (cryo-EM), where molecules are imaged in an electron microscope, is a molecular imaging method and gained a lot of attention in recent years. Due to groundbreaking improvements regarding hardware and data processing, the field of research has highly improved. In 2017, pioneers in the field of cryo-EM got the Nobel Prize in Chemistry¹. Today, using cryo-EM many molecular structures can be observed with near-atomic resolution. The big challenge with cryo-EM is enormous noise.

TODO: Introduce CT and cryo-EM

ToDo:Reference to Results

ToDo: Overview of chapters

¹ <https://www.nobelprize.org/prizes/chemistry/2017/press-release/>

2

Molecular Imaging methods

In current chapter molecular imaging methods *computed tomography* and *cryo-electron microscopy* (cryo-EM) will be introduced. Further, their observation model is defined in a mathematic way and reconstruction is presented. Application of cryo-EM is a major motivation for the Master Thesis, as the problem is not easy to solve due to dealing with enormous noise and unknown observation angles. Computed Tomography is a similar problem, but slightly simpler as problem can be in 2D, and is therefore well suited as a first step to make an algorithm work for cryo-EM.

2.1 Computed tomography

Computed tomography (CT) is a well established molecular imaging method. Using X-ray source, fan shaped beams are produced which scan the imaging object, resulting in many observations taken over straight lines [2].

Tomography reconstruction: Tomographic reconstruction [5] is a popular inverse problem. The aim is to reconstruct an imaged object from observed observations. The reconstruction object can be in two-dimension (2D) or in three-dimension (3D).

The focus in computed tomography during the Thesis will be on the 2D case, which is called *classical tomography*.

2D tomographic observation: Mathematically, observations are defined as follows:

$$\begin{aligned} y_i[j] &= p_i + \eta_i[j], \text{ with } 1 \leq i \leq N \text{ and } 1 \leq j \leq M, \\ &= R(x, \theta_i, s_j) + \eta_i[j], \end{aligned} \quad (2.1)$$

with

- N : number of observations
- M : observation dimension
- $y_i \in \mathbb{R}^M$: i -th observation with $y_i[j] \in \mathbb{R}$: j -th element of observation
- $p_i \in \mathbb{R}^M$: i -th noiseless observation with $p_i[j] \in \mathbb{R}$: j -th element of noiseless observation
- $x \in L^2(\Omega)$: original object with $\Omega \subset \mathbb{R}^2$ and L^2 : Lebesgue space
- $R(\cdot; \theta, s) : L^2(\Omega) \rightarrow L^2(\tilde{\Omega}), x \mapsto R(x; \theta, s)$: Radon Transform [19] with, $\tilde{\Omega} \subset \mathbb{R}$, $\theta_i \in \mathbb{R}$: observation angle and $s_j \in \mathbb{R}$: sampling point
- $\eta_i \in \mathbb{R}^M$: Gaussian noise with $\eta_i[j] \sim \mathcal{N}(0, \sigma^2) \in \mathbb{R}$

During Thesis, the notation p for noiseless observation and y for observation with noise is used. In practice, p is not observable directly and observed signal y needs to be denoised. Further, x is used for original object.

Data of Radon Transform is often called a *sinogram*. In figure 2.1(a) the Shepp-Logan phantom can be seen. It is often used as an image for simulating a brain CT. Further, in figure 2.1(b) and figure 2.1(c) observation sinograms can be seen with and without noise respectively. To apply Radon Transform, parameter θ and s need to be specified. In this case, $\theta \in \mathbb{R}^{500}$ was evenly spaced between $[0, 2\pi]$ and $\dim(s) = 400$. With these parameters, $p \in \mathbb{R}^{500 \times 400}$ and p can be plotted as image with resolution 500x400. Further, noise was added to reach a signal-to-noise-ratio (SNR) of 10dB.

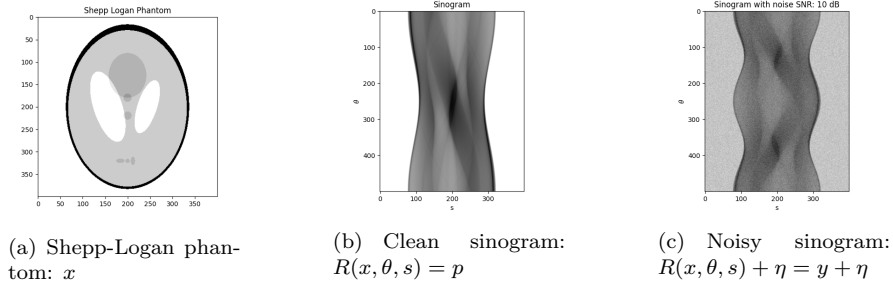


Figure 2.1: Shepp-Logan phantom and sinograms

Filter Backprojection: Filter Backprojection [5] (FBP), is a reconstruction method, typically used in classical tomography. It allows to inverse the Radon Transform and enables reconstruction of the original object x . It can be defined as:

$$FBP(\cdot; \theta, s) : L^2(\tilde{\Omega}) \rightarrow L^2(\Omega), y \mapsto FBP(y; \theta, s), \quad (2.2)$$

with θ as projection angles and s sampling points. The algorithm fails when working with noisy data [16].

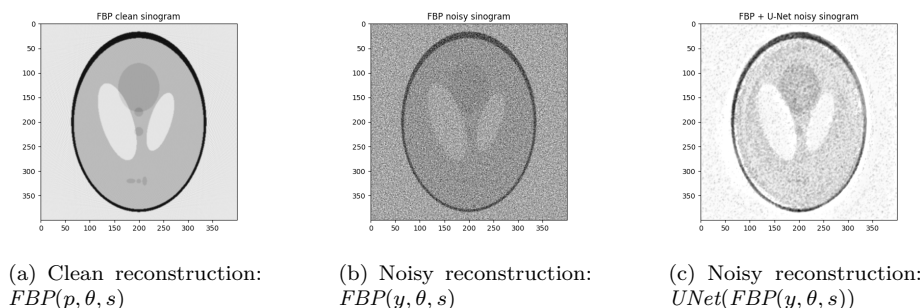


Figure 2.2: Shepp-Logan FBP reconstructions

In figure 2.2(a) and figure 2.2(b) reconstruction can be seen from Shepp-Logan phantom sinogram (figure 2.1(b)) and its noisy version (figure 2.1(c)). The quality of noisy reconstruction is rather low, some important details are missing, and the noise dominates reconstruction. If more noise is present in y , reconstruction will be of even lower quality.

U-Net Leuschner et al. [14] compared different reconstruction methods for computed tomography. Today’s state-of-the-art reconstruction algorithms are Deep-Learning based. U-Net[15], a convolution neural network approach, performed much better than only applying FBP, especially when dealing with noise.

During practical part of the Thesis, U-Net was used and trained on lodopab-ct dataset [13], a brain CT dataset. More details on U-Net and how it was used can be found in chapter 4 *GAT-Denoiser* and chapter 5 *Results*. In figure 2.2(c), reconstruction using FBP and U-Net can be seen. Quality of reconstruction is still not perfect, but overall noise is drastically decreased.

2.2 Cryo-EM

Cryo-EM is another molecular imaging method, that enables the view of molecules in near-atomic resolution. In the Master Thesis, only single-particle cryo-EM [8] is considered, when writing about cryo-EM it always refers to single-particle cryo-EM.

During imaging process molecules are frozen in a thin layer of ice, where they are randomly oriented and positioned. Random orientation and positioning makes reconstruction challenging, but freezing allows observation in a stable state where molecules are not moving. With an electron microscope, two-dimensional tomographic projection images of molecules

in the ice are observed, which are called *micrograph*. Frozen molecules are fragile, and electron microscope needs to work with very low power (electron dose), resulting in highly noisy images. The resulting (SNR) is typically smaller than 1, which indicates that there is more noise than signal [16].

Further, observed molecules are not equal in the sense that there are some structural varieties between molecules (isotopes). While observing same molecule in ice many times, single observation could be from different isotopes.

3D cryo-EM reconstruction: Similar to tomographic reconstruction, cryo-EM reconstruction problem [1] is defined. It can be seen as a 3D reconstruction problem as the original object $x \in L^2(\Omega)$ to be reconstructed is in 3D. Based on many observed micrographs, collected by the electron microscope, the original object x will be estimated.

Cryo-EM reconstruction is computational intensive and multiple steps are needed to get from observed, raw data to the final structure [8].

3D cryo-EM observation: Mathematically, observation is defined as follows:

$$\begin{aligned} y_i &= p_i + \eta_i, \text{ with } 1 \leq i \leq N, \\ y_i &= \Pi_z(\text{Rot}(x; \theta_i)) + \eta_i, \text{ with } 1 \leq i \leq N, \end{aligned} \quad (2.3)$$

where

- N : number of observations
- M : observation dimension
- $y_i \in \mathbb{R}^M$: i -th observation with $y_i[j] \in \mathbb{R}$: j -th element of observation
- $p_i \in \mathbb{R}^M$: i -th noiseless observation with $p_i[j] \in \mathbb{R}$: j -th element of observation
- $x \in L^2(\Omega)$: original object with $\Omega \subset \mathbb{R}^3$ and L^2 : Lebesgue space
- $\Pi_z : L^2(\Omega) \rightarrow L^2(\tilde{\Omega}), x \mapsto \int x(\cdot, \cdot, z) dz$: Z-axis projection operator, with $\tilde{\Omega} \subset \mathbb{R}^2$
- $\theta_i = [\theta_i^{(1)}, \theta_i^{(2)}, \theta_i^{(3)}]$: 3D rotation matrix with $\theta_i^{(1)}, \theta_i^{(2)}, \theta_i^{(3)} \in \mathbb{R}$ and $R_{\theta_i} = R_{e_x}(\theta_i^{(1)})R_{e_y}(\theta_i^{(2)})R_{e_z}(\theta_i^{(3)}) = [R_{\theta_i}^1, R_{\theta_i}^2, R_{\theta_i}^3] \in SO(3)$ (see A.2 for further details)
- $\text{Rot} : L^2(\Omega) \rightarrow L^2(\Omega), \text{Rot}(x, \theta_i) = ((x_1, x_2, x_3) \mapsto x(x_1 R_{\theta_i}^1, x_2 R_{\theta_i}^2, x_3 R_{\theta_i}^3))$: rotation operator
- $\eta_i \in \mathbb{R}^M$: Gaussian noise with $\eta_i[j] \sim \mathcal{N}(0, \sigma^2) \in \mathbb{R}$

As y_i is not observable directly, discretization is needed:

$$\begin{aligned} y_i &= (\Pi_z(\text{Rot}(x; \theta_i)) + \eta_i)(\Delta), \text{ with } 1 \leq i \leq N \\ y_i[j, k] &= \Pi_z(\text{Rot}(x; \theta_i))_{j, k} + \eta_i[j, k], \text{ with } 1 \leq i \leq N \text{ and } 1 \leq j, k \leq M, \end{aligned} \quad (2.4)$$

where

- $\Delta \subset \tilde{\Omega}^{M^2}$: sampling grid with dimension M^2
- Further, $y[j, k]$, $\eta[j, k]$ and $\Pi_z(\cdot)_{j,k} \in \mathbb{R}$ with j, k as indices of the sampling grid.

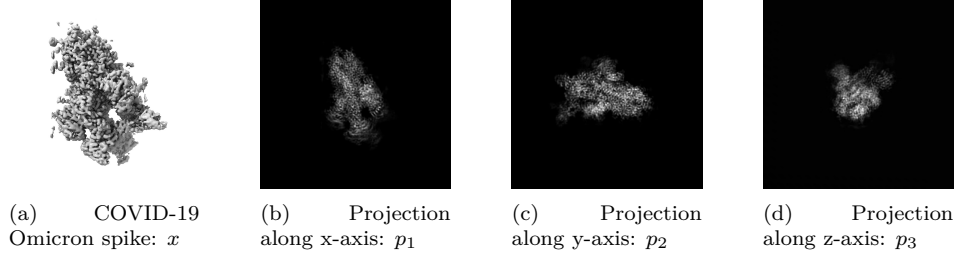


Figure 2.3: Cryo-EM reconstruction and clean projections of COVID-19 Omicron spike ²

Extended formula: Equation 2.3 is a simplified version of cryo-EM. First, point spread function (PSF) of the microscope is not taken into account. Secondly, structural variety is ignored, the underlying object x is not the same for every observation as modelled in the equation. Precisely, x can be seen as a random signal from an unknown distribution defined over all possible molecules structures.

The equation can be extended and defined as the following:

$$y_i = h_i \circ \Pi_z(\text{Rot}(x_i; \theta_i)) + \eta_i, \text{ with } 1 \leq i \leq N \quad (2.5)$$

where h_i is the PSF of the microscope and \circ defines the convolution. Further, $x_i \in X$ where X is the set of all possible molecule structures.

Difference to tomographic reconstruction: The problems are highly related, but cryo-EM reconstruct is more challenging. While CT observation, patient is asked to not move and therefore, angles of projections are known. Whereas, in cryo-EM, this information will be lost during freezing. Secondly, high level of noise makes cryo-EM much more challenging.

2.3 Abstract form

Observation: As tomographic reconstruction and cryo-EM reconstruction are rather similar, goal of the Master Thesis will be to design an algorithm, that can be applied in both scenarios.

Therefore, an abstract form of the problems will be defined in the following. First, a similar notation as before is used, but in a more general way with $x \in L^2(\Omega)$ where $\Omega \subset \mathbb{R}^D$ with D as the dimension of the space of original object and $\tilde{\Omega} \subset \mathbb{R}^{D-1}$ as the dimension of the space of observations.

$$\begin{aligned} y_i &= p_i + \eta_i(\Delta), \text{ with } 1 \leq i \leq N \\ y_i &= (A(x, \theta_i) + \eta_i)(\Delta), \text{ with } 1 \leq i \leq N \end{aligned} \quad (2.6)$$

where,

- N : number of observations
- M : observation dimension
- $y_i \in \tilde{\Omega}^M$: the i -th observation
- $p_i \in \tilde{\Omega}^M$: the i -th noiseless observation
- $x \in L^2(\Omega)$: original object
- $A : L^2(\Omega) \rightarrow L^2(\tilde{\Omega}), x \mapsto A(x; \theta_i)$: a non-linear operator
- $\theta_i \in \mathbb{R}^P$: projection angle vector, with P projection dimension
- $\eta \sim \mathcal{N}(O, \sigma^2 I) \in \tilde{\Omega}^M$: Gaussian noise
- $\Delta \subset \tilde{\Omega}^M$: term for discretization

Reconstruction: Further, an abstract form of the reconstruction operator is defined as

$$Recon : L^2(\tilde{\Omega}) \rightarrow L^2(\Omega), y \mapsto Recon(y; \theta)(\Delta) \quad (2.7)$$

with

- $\theta_i \in \mathbb{R}^P$: projection angle vector, with P projection dimension
- $\Delta \subset \tilde{\Omega}^D$: term for discretization, D as the dimension of the space of original object

Check: Theta and discretization term

Classical tomography: Classical tomography parameters are defined with $D = 2, P = 1$. Further, $A(\cdot)$ is the Radon Transform (see equation 2.1). Reconstruction operator can be defined as FBP (with or without U-Net[15]).

Cryo-EM: Cryo-EM parameters are defined with $D = 3$ and $P = 3$ as θ_i not only corresponds to a projection angle vector but also some rotation. Further, $A(\cdot)$ can be defined as $\Pi_z (Rot(x; \theta))$ where Rot is the 3D rotation and Π_z the tomographic projection.

High noise regime: Cryo-EM observations are highly noisy, which makes reconstruction challenging. There are different ways to reduce noise from observations, most of them are related to averaging. Averaging need to consider similar observations and ignore diverse ones. In the defined abstract model, averaging over paired observations from θ should be a good averaging model. But how can it be achieved?

One idea would be to measure distances between observation. Another way is to find a low-dimensional embedding which maps our observations y to some θ . When talking from low-dimensional embeddings, there is no way around Graph Learning, which will be introduced in the following chapter 3 *Graph Denoising*.

3

Graph Denoising

The following chapter establishes connection between graphs and denoising in high-noise domains, such as cryo-EM. First, a broad definition of graphs is given and further, the term "Graph Denoising" is introduced and explained. Finally, connection to Graph Laplacian, Manifolds and molecular imaging methods is established.

3.1 Graph Foundations

Real world data can be in graph structure, like social networks, citation networks, protein interaction networks or google search. If data is not available in graph structure, a graph can be artificially constructed with methods like k-nearest neighbors (k-NN) or others. A general framework for graph construction is introduced in section 3.1.2 *Graph construction*.

Graph Learning: Graph Learning is a prominent research area and got a lot of attention in recent years. It is a way of applying ML on graphs and algorithms emerged from ML but also other fields. When a graph is available, one can start using Graph Learning algorithms for solving tasks. Popular tasks are *node classification* or *link prediction*, where a model is learned from node and edge features as well as topology. The model can then be used for prediction or classification on nodes or edges. Another common task is *community detection*, where the aim is to identify cluster of nodes within the input graph. Further, graphs are highly favored for *dimensionality-reduction*, where graph algorithms provide a helpful tool, as ordinary algorithms like principal component analysis fail to establish a meaningful dimensionality reduction.

3.1.1 Graph definition

A graph is defined as $G = \langle V, E \rangle$, where V is a set of vertices (or nodes) and E is a set of edges (or links). Edges are defined as a set of tuples (i, j) , where i and j determine the index of vertices in the graph.

Graph properties: A graph can be either *directed* or *undirected*. In a directed one, an edge connects explicitly from one node to another, which means that edge $(i, j) \neq (j, i)$. In

undirected graphs, edges have no direction and ordering does not matter, therefore $(i, j) = (j, i)$.

The *neighborhood*, denoted by $\mathcal{N}(i)$, of a node i is defined as all adjacent nodes. In other words, there is an edge between neighborhood nodes and i . Further, edges can have *weights*, which is a method to define importance to neighbors, resulting in a *weighted* graph. *Degree* of a node are the number of incoming edges.

Adjacency matrix: To do calculations with graphs, it is common to translate graphs in a matrix, such as the adjacency matrix. The (binary) adjacency matrix of graph $G = \langle V, E \rangle$ is defined as follows:

$$A_{ij} = \begin{cases} 1 & \text{if } (i, j) \in E \\ 0, & \text{otherwise} \end{cases} \quad (3.1)$$

Matrix A has dimension $\mathbb{R}^{N \times N}$ with N as number of nodes and indices of A correspond to nodes in V . If there exists an edge between two nodes, entry in A will be set to 1, otherwise to 0. This leads to an unweighted graph, as weights of all edges will be 1, but could easily be extended by assigned not just values of 1 or 0. When G is undirected, corresponding adjacency matrix will be symmetric. Eigenvalues of A are called *spectrum* of G .

3.1.2 Graph construction

When data is not available as a graph, it can be easily constructed. Consider data from space $\Omega \subset \mathbb{R}^M$, but could basically be any arbitrary space. Then, each node is associated with some element $v \in \Omega$. Further, graph G can be constructed by using:

$$A_{ij} = \begin{cases} 1 & \text{if } \text{dist}(v_i, v_j) < \tau \\ 0, & \text{otherwise} \end{cases} \quad (3.2)$$

, where v_i, v_j are nodes from indices i and j , *dist* corresponds to a similarity (or distance) measure and τ is a threshold, when to consider two nodes to be adjacent. K-NN is one possible implementation of a graph construction algorithm, where for every node, k neighbors will be defined. The neighborhood \mathcal{N}_i of v_i is defined as k nodes with the smallest similarity measure.

Noisy observations: But what happens if our data is noisy? Consider measurements which will give access to $y = p + \eta$, where $y, p \in \Omega$ and noise η is assumed to be drawn from Gaussian distribution $\mathcal{N} \sim (0, \sigma^2)$. y refers to the noisy observation and p to noiseless observation. While constructing a graph, nodes are associated with elements from p ($\text{dist}(p_i, p_j)$) in the noiseless case and from y ($\text{dist}(y_i, y_j)$) is the noisy case. Therefore, k-NN applied on noisy data, is assumed to connect some nodes wrongly, as distance measure *dist* is not accurate due to noise. It is expected that the more noise is available in data, the more nodes are wrongly connected with k-NN.

Constructing Graphs for molecular-imaging: For a molecular-imaging (cryo-EM or computed tomography) observation, a graph can be constructed as well. Every observation

y_i can be assigned to a node v_i , which means that $V \subset \mathbb{R}^M$, where M is again observation dimension. Further, $|V| = N$ where N is the number of observations, which defines how many projections from different angles θ are within the observation.

As nodes are defined, it is time to have a look at edges. To apply equation 3.2 similarity measure *dist* needs to be defined. For computed tomography, a distance measure between observations can be set up by using the ℓ_2 -norm $\|y_i - y_j\|$. For cryo-EM it is more challenging, as projections are drawn with some random 3D rotation and projection, it can happen that two samples are equivalent up to 2D rotation. Consider a first observation y_1 , which has no 3D rotation and a second observation y_2 with a rotation in x-y plane by 45° . The two projections have a defined in-plane rotation g , such that $g y_1 = y_2$. Therefore, a term of in-plan rotation is added to the ℓ_2 -norm: $\min_{g \in SO(1)} \|g y_i - y_j\|$, which is inspired by [9]. Now, everything is available to create a graph from a molecular-imaging observation.

3.2 Graph Denoising definition

First, *Graph Denoising* is not a common term in literature. In previous section, graphs based on noisy observations were introduced and goal is to denoise these graphs, which means to estimate original graph G from a given noisy graph G_0 . This is our definition for Graph Denoising, which is rather related to signal or image denoising. Reconstruction of a true signal given noisy observation signal is done via averaging, that can be performed locally, by the calculus of variations or in the frequency domain[3].

Noisy Graph: For every noisy graph there exists an original graph $G = \langle V, E \rangle$. The noisy graph G_0 can further be defined as $G_0 = \langle V, E_0 \rangle$, where $E_0 = E \setminus E_0^- \cup E_0^+$ with $E_0^- \subseteq E$ and $E_0^+ \cap E = \emptyset$.

G_0 consists of same nodes V as original graph G . From E some edges are removed (denoted by E_0^-) and some are added (denoted by E_0^+), which results in edges E_0 .

Graph Denoising can therefore be written as

$$GD : A_0 \mapsto \tilde{A} \approx A \quad (3.3)$$

, where A_0 , \tilde{A} , A denotes adjacency matrix from noisy input graph, denoised graph and original graph respectively.

Connection to link prediction: Link prediction is a task in Graph Learning. The goal is to predict existence of a link between two nodes. The task can be formulated as a missing value estimation task. A model M_p is learned from a given set of observed edges. The model finally maps links to probabilities $M_p : E' \rightarrow [0, 1]$ where E' is the set of potential links.

Further, U determines the set of all possible vertices of G , therefore $E \subseteq U$. Clearly, Graph Denoising can be seen as a link prediction problem. The difference is, that in link prediction a model from a set of observed links is learned $E' \subseteq E$ and in Graph Denoising model is learned from $E' \subseteq U$.

One could also say that link prediction problems are a subset of graph denoising problems.

3.2.1 Non-local means:

In the following section, a short introduction to the state-of-the-art image denoising method non-local means is given [3]. For a given noisy image v , the denoised image is defined as $NL[v](i) = \sum w(i, j) v(j)$, where $w(i, j)$ is the weight between pixel i and j . Weight can be seen as similarity measure of pixels, which are calculated over square neighborhoods. Similar pixel neighborhoods have a large weight and different neighborhoods have a small weight. More general, denoised image pixel i is computed as a weighted average of all pixels in the image, therefore, in a non-local way.

Non-local means is not a denoising algorithm, which works with graph as a data structure. But, it uses a neighborhood for averaging, which shows great potential for graph as a data structure for denoising, as graphs can represent neighborhoods really well.

3.3 Graph Deep Learning

As already mentioned, Graph Denoising can be seen as a way of link predication. The state-of-the-art method for solving link prediction are *Graph Deep Learning* approaches. Graph Deep Learning is a fast evolving field in research. With Graph Neural Networks (GNN) [11] the framework for neural networks with graphs has been established.

Using Graph Convolutional Networks (GCN) [12] for graph feature extraction is a popular way. With GCN a new feature representation is iteratively learned for node features (edge features are not considered). It can be seen as an averaging of nodes over their neighborhood where all neighbors get the same weight combined with some non-linear activation (e.g. ReLu). To consider node itself in averaging, [12] apply the so-called "Renormalization trick", where self-loops are added to the adjacency matrix and after every layer, a normalization step is applied. The topology of the graph will not be adjusted during learning process.

Veličković et al. [21] extended the concept of GCN with attention and not all neighboring nodes get the same weight (attention). Simple Graph Convolutional Network [24] proposed a simplified version of GCN. They could verify their hypothesis that GCN is dominated by local averaging step and non-linear activation function between layers do not contribute too much to the success of GCN. Therefore, it can be seen as a way of power iteration (see A.3 *Power Iterations* for further information) over the adjacency matrix with normalization in every layer. Wang et al. [23] proposed an extension to GCN by not operating on the same graph in every layer but adopting underlying graph topology layer by layer.

3.4 Graph Laplacian & Manifolds

3.4.1 Graph Laplacian

Graph Laplacian (GL) is a matrix that represents a graph and can be used to find many important properties. It is a very powerful tool and a good introduction and overview can be found by [18, 22].

GL is defined as follows:

$$L = D - A, \quad (3.4)$$

where A is the adjacency matrix and D the degree matrix (diagonal matrix with degree of nodes as entries).

3.4.2 Manifolds

In high-dimensional data Euclidean distances are not meaningful, in the sense that they will not capture similar data points well. One is looking for a geodesic distance, representing the shortest path of two point on a surface. Graph Laplacian can be used to compute a *Manifold*, which can help in such scenarios. In manifold space, Euclidean distances make sense again. Let manifold M be defined as $\mathcal{M} = \{f(x), f \in C^K, f: \mathbb{R}^D \rightarrow \mathbb{R}^d\}$. Manifolds are a well established mathematical concept. In the Master Thesis, only C^k differentiable d -dimensional manifolds defined by \mathcal{M} are considered. When $d \ll D$, manifolds define a *low-dimensional embedding*, which maps from high-dimensional space \mathbb{R}^D to low-dimensional space \mathbb{R}^d .

Let's give two popular examples of manifolds, namely *circle* and *sphere*. The circle is a 1D manifold, where $d = 1$ and $D = 2$. A sphere is a 2D manifold, with $d = 2$ and $D = 3$. In figure 3.1(a), 200 samples are drawn from a uniform distribution of unit-circle manifold and in figure 3.1(b), 800 samples are drawn from a uniform distribution of unit-sphere manifold, as well as the sphere itself.

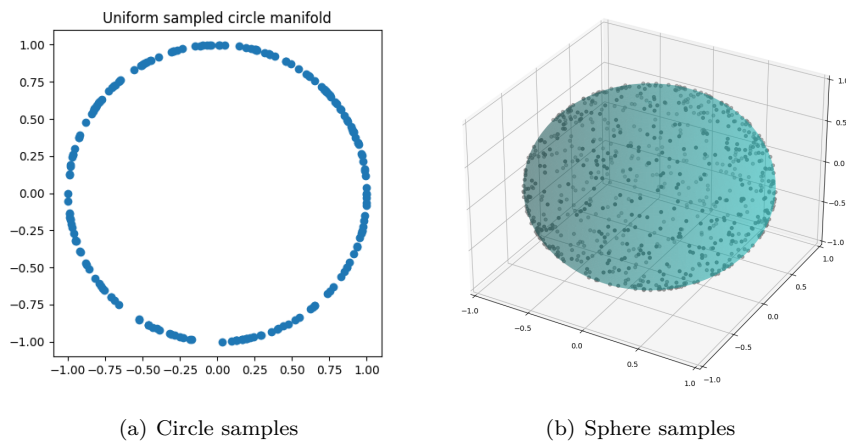


Figure 3.1: Samples drawn from 1D and 2D manifold.

One popular algorithm for calculating manifolds is diffusion maps [6], which is a non-linear

approach for calculating low-dimensional manifolds for (high-dimensional) datasets, using Graph Laplacian. Vector diffusion maps [17] generalize the concept of diffusion maps for vector fields. Multi-frequency vector diffusion maps [9] can be seen as an extension to vector diffusion maps, which works well even on highly noisy environments. Fan and Zhao [10] successfully applied multi-frequency vector diffusion Maps in cryo-EM setting, where it was used for denoising purpose.

3.4.3 Manifold assumption

Manifold assumption is a popular assumption for high-dimensional datasets. For a given dataset in high-dimension, one can assume that data points are samples drawn from a low-dimensional manifold, that embeds the high-dimensional space. Therefore, if underlying manifold can be approximated, a dimensionality reduction is established as one can embed data points in the low-dimensional manifold space. There is a complete area of research devoted to this manifold assumption called Manifold Learning[4].

3.4.4 GL-manifold calculation

A simple low-dimensional embedding (manifold) of a dataset can be calculated with Graph-Laplacian by the following:

1. Construct k-NN graph from observations (see section 3.1.2 *Graph construction*).
2. Calculate the (normalized) Graph Laplacian (see equation 3.4).
3. Extract the second, third (and fourth) the smallest eigenvectors.

3.4.5 Manifold of computed tomography and cryo-EM

As a tool for GL-manifold calculation is established, it can be observed how the GL-manifold of classical tomography and cryo-EM objects look like. In the following, Shepp-Logan phantom is again used as an example of classical tomography and the low-dimensional embedding is calculated from sinogram, following instructions from section 3.4.4 *GL-manifold calculation*.

Radon Transform, parameters θ and s where specified as $\theta \in \mathbb{R}^{500}$ as evenly spaced between $[0, 2\pi]$ and $\dim(s) = 200$.

In figure 3.2(a), GL-manifold calculated from clean sinogram and $k = 2$ can be seen. GL-manifold looks like a perfect circle. Further, noise was added to the sinogram to reach SNR 20dB and GL-manifold was computed with $k = 2$, which failed (figure 3.2(b)). But, if neighborhood is not too strictly defined and k is increased to 4, GL-manifold looks more circle like again (figure 3.2(c)).

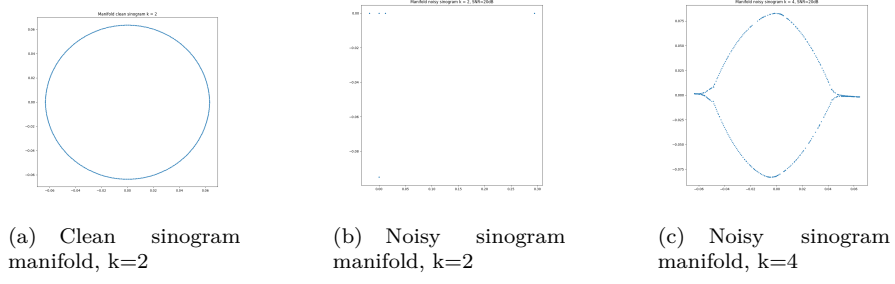


Figure 3.2: Shepp-Logan phantom sinogram manifolds.

In the field of classical tomography and cryo-EM, underlying low-dimensional GL-manifold is well-defined for none-noisy data. In the 2D case of classical tomography, underlying GL-manifold is a circle, whereas in 3D case of cryo-EM GL-manifold is defined as a sphere. This fact can be exploited during learning.

Manifold quality: Finding a good GL-manifold is not easy and in our case, GL-manifold is dependent on parameter k during graph construction as well as parameter θ , s and η for obtaining the sinogram.

K is an important parameter for building up a graph. If set too low, neighbors do not capture similar data well as too few nodes are connected. Further, if k is set too high, strength of a neighbor is weakened and data is not well explained as well. In figure 3.3(a), GL-manifold computed by clean sinogram and k from 2 to 10 is illustrated. One can see, that from $k \leq 4$ GL-manifold results in a perfect circle and with $k > 4$ is moves further away from the circle.

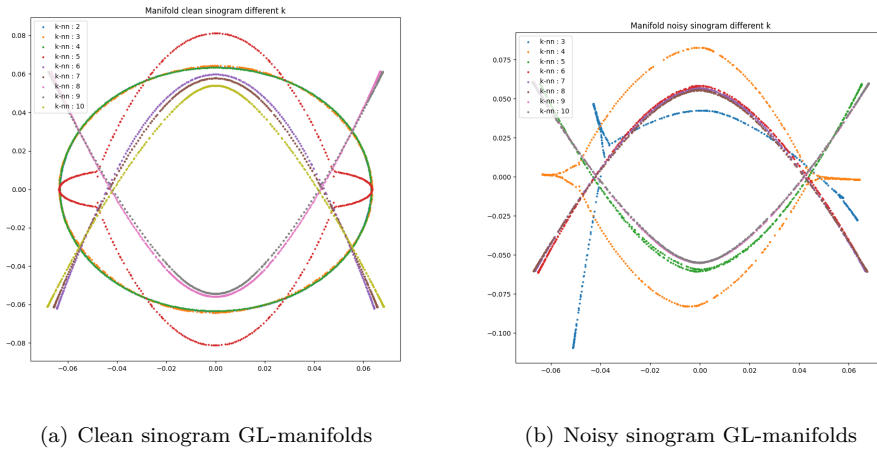


Figure 3.3: Shepp-Logan phantom sinogram manifolds.

If data is noisy, it is expected to be harder to construct a meaningful GL-manifold, as

some connections within the graph will be noisy. This is exactly what is illustrated in figure 3.3(a), where different GL-manifold for noisy sinogram (SNR=20dB) and k from 3 to 10 are illustrated. GL-manifold can never express the true data with a perfect circle. As noise is chosen rather moderate, GL-manifold has still some power to express underlying data and is expected to decrease, if noise is increased.

Further, when observing a sinogram, parameter θ defines how many observations (straight lines) are drawn and $\dim(s)$ defines the amount of sampling points. Both have great impact to expressiveness of our sinogram.

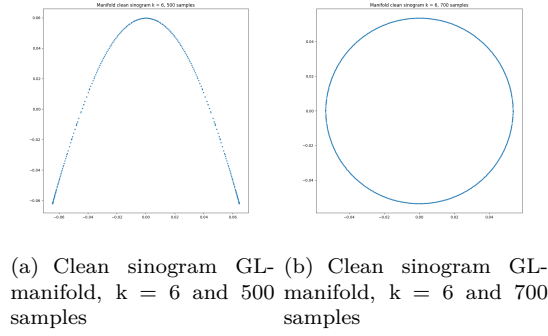


Figure 3.4: Shepp-Logan phantom sinogram GL-manifolds: Importance of number of samples.

In figure 3.4(a) GL-manifold with $\theta \in \mathbb{R}^{500}$ and $k=6$ is illustrated for clean sinogram. It looks like 6 are too many neighbors, as the perfect circle cannot be established anymore. But, if θ is increased $\theta \in \mathbb{R}^{700}$, more nodes are available to choose good neighbors from and a perfect circle can be established (figure 3.4(b)).

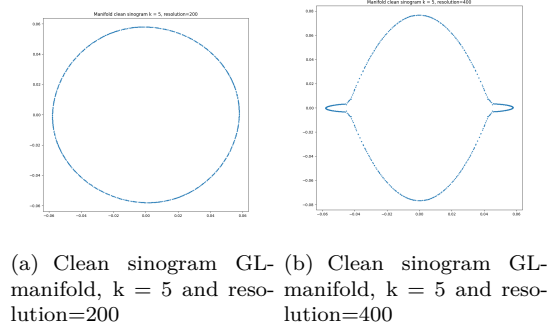


Figure 3.5: Shepp-Logan phantom sinogram GL-manifolds: Importance of number of samples.

Moreover, the number of sampling points is important as well. Here, for more sampling points it is expected to be harder to come up with good neighbors (fixing k and number of samples), as more data need to be explained with the same amount of samples and neighbors, and it is more likely, that nodes are connected wrongly. This can be seen in figure 3.5(a)

and figure 3.5(b), where with $\dim(s) = 200$, the perfect circle can be established and with $\dim(s) = 400$, not anymore (by same parameter $k = 5$ and $\theta \in \mathbb{R}^{500}$).

As with the last plots illustrated, the GL-manifold is pretty sensitive. Therefore, it is best practice to try different parameters (k) for finding the best GL-manifold.

TODO: Connection to next chapter

4

GAT-Denoiser

In the current chapter, contribution during Master Thesis is presented. As result, a GNN can be presented which is called *GAT-Denoiser*. Its main components and overall architecture is introduced. The focus during practical part was on classical computed tomography in 2D but can be generalized to cryo-EM and 3D.

Goal: As introduced in chapter 2 *Molecular Imaging methods*, molecular imaging methods computed tomography and cryo-EM are the problems to approach. Further, high-noise regime is the domain of interest, to be more precise SNR between $[-10, 0]$. For a given set of observations (many sinograms or micrographs), a GNN will be trained, such that it enables denoising of observations which are expected to have a better reconstruction result after denoising. Trained model allows to denoise not seen observations which are from the same family of observations.

To start solving the problem, an algorithm was designed to work with computed tomography, additionally projection angles are assumed to be known and θ was defined as equally spaced in the interval $[0, 2\pi]$.

Input graph: To recap from section 3.1.2 *Graph construction*, a graph constructed from molecular-imaging observation will have single observations as nodes (one horizontal line of the sinogram). As θ is fixed, angle corresponding to each single observation are known. Based on these angles, neighboring nodes can be connected.

For GAT-Denoiser, this entails that graph topology is fixed and a k-NN graph can be constructed from θ .

4.1 Concept

In the following section, the concept of GAT-Denoiser is introduced. GAT-Denoiser is a GNN and has two main components, namely convolution layers and GAT layers. The main

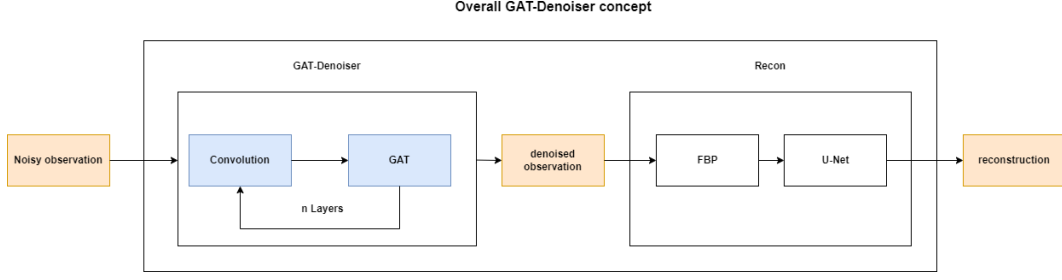


Figure 4.1: GAT-Denoiser concept

idea of GAT-Denoiser is to enable denoising of observations:

$$GAT-Denoiser(\cdot) : L^2(\tilde{\Omega}) \rightarrow L^2(\tilde{\Omega}), y \mapsto GAT-Denoiser(y) \quad (4.1)$$

Input y of GAT-Denoiser is a noisy observation, output will be a denoised version of it. GAT will be responsible to average over observation neighbors and convolution to denoise single observations. For every GAT layer there is a preceding convolution. In the case of computed tomography, this will be 1D convolution and for cryo-EM a 2D convolution.

The GAT is expected to denoise observation signal with its neighbors by averaging. Further, convolution is added to denoise single observations.

But, the main overall goal is to get the best possible reconstruction from noisy observation y which approximates original object x and not just denoise observation y which approximates noiseless observation p .

$$x \approx Recon(GAT-Denoiser(y)), \quad (4.2)$$

with $Recon : UNet(FBP(\cdot))$

Therefore, an end-to-end learning approach is used where quality of reconstruction is compared during GAT-Denoiser training, which is expected to perform better than only optimizing denoising of observations.

In figure 4.1 overall GAT-Denoiser concept is illustrated.

K-hop neighborhood: In GNNs, multiple layers expose the k-hop neighborhood. So for a network with k layers, network operates on the k -hop neighborhood. In GAT-Denoiser, this corresponds to the layers of GAT. Therefore, if writing from one layer, it is referring to convolution and GAT together.

4.2 Components

In the following, the three main components are explained individually and in section 4.3 *Architecture* connected to GAT-Denoiser architecture in more detail.

4.2.1 Graph Attention Networks

The main component of GAT-Denoiser is a GAT. As mentioned in section 3.3, GAT is an extension to GCN and adds attention (or weights) to neighbors for learning new node feature representations. Again, topology of the graph will not change but weighted averaging over the neighborhood will take place and this is what in denoising is a good idea.

Single Layer Input of a single GAT layer are node features $h = \{h_1, h_2, \dots, h_N\} \in \mathbb{R}^F$, where N is the number of nodes and F the number of features per node. Single layer will map input to output, which can potentially have different dimensions: $h' = \{h'_1, h'_2, \dots, h'_N\} \in \mathbb{R}^{F'}$. As is other GNNs, input features are initially linearly transformed and parametrized by a learnable weight matrix $W \in \mathbb{R}^{F' \times F}$. This allows to add enough expressiveness to the neural network and weights are learned during training. Further, attention coefficients are computed, which indicates importance of node j to node i :

$$e_{ij} = a(Wh_i, Wh_j), \quad (4.3)$$

with a as the shared attentional mechanism $a : \mathbb{R}^{F'} \times \mathbb{R}^{F'} \mapsto \mathbb{R}$. But how to define the attentional mechanism? Veličković et al. [21] proposed to use a single-layer feedforward neural network, parametrized by a weight vector $a \in \mathbb{R}^{2F'}$ and LeakyReLU as activation function.

To compare coefficients e across different nodes, normalization is needed. Therefore, softmax is used as normalization $\alpha_{ij} = \text{softmax}_j(e_{ij})$ such that all attention coefficient of one node sum up to 1 and therefore are nicely comparable across nodes. Finally, new node embedding is calculated as:

$$h'_i = \sigma \left(\sum_{j \in \mathcal{N}_i} \alpha_{ij} Wh_j \right), \quad (4.4)$$

with σ as some arbitrary activation function.

Multi-Head attention Motivated by Vaswani et al. [20], multi-head attention can be beneficial to stabilize learning process. Therefore, not only a single weight matrix is learned, but W is split up in several parts, all learned individually:

$$h'_i = \parallel_{k=1}^K \sigma \left(\sum_{j \in \mathcal{N}_i} \alpha_{ij}^k W^k h_j \right), \quad (4.5)$$

where \parallel corresponds to concatenation, α_{ij}^k the k -th attention mechanism and W^k the linear transformations weight matrix. The final output consists of KF' output features.

Last layer: As in the last layer, dimension need to be corresponding to output dimension, concatenation is no longer plausible and averaging is used to match desired dimension.

4.2.2 Convolution

The second key component of GAT-Denoiser is convolution. Convolution is an important part in Signal Processing, if not the most important one. It allows to average an incoming signal, further, it is very popular in computer vision. Convolution commonly operators on pixel spaces, where every observation location or time slot gets one value assigned.

$$x \star k = y, \quad (4.6)$$

where x is input signal, k is kernel, \star the convolution operator and y the convolved signal. To apply convolution, a kernel with weights needs to be defined. This kernel will then slide over the input signal x and computes the dot product with its weights. In figure 4.2.2 an illustration of 1D convolution can be seen. In this example, kernel size is set to 3, n refers to input signal dimension and m to output signal dimension. In the example $n = m + 2$, so the convolved output signal will be decreased by 2. The concept of convolution can be extended to arbitrary dimensions.

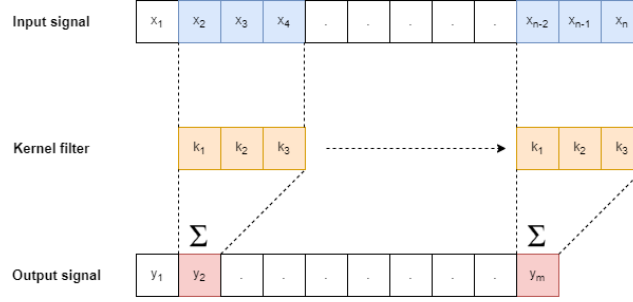


Figure 4.2: 1D Convolution

Padding: can be defined to add pixels to boundary of the signal. In the example, padding is set to 0 and therefore, the signal dimension is decreased by 2. If signal dimension should be fixed during convolution, padding is a powerful tool. For padding 1, the input dimension n would be equal to output dimension m , as an extra element in the output signal will be at convolved at boundaries.

Stride: is the parameter how far kernel moves each time. In the example, stride was defined to be 1. If stride is increased, the output signal dimension will decrease.

4.2.3 U-Net

U-Net can boost performance of computed tomography reconstruction and is therefore our third component in GAT-Denoiser. It is a convolutional neural network, which is well suited for image segmentation in different domains. [15] showed great success for biomedical image segmentation.

The neural network architecture consists of contracting path and expansive path, resulting in a U-shape, as illustrated in figure 4.2.3.

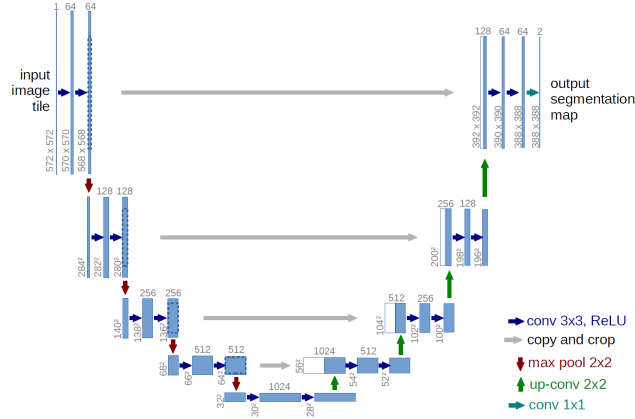


Figure 4.3: U-Net architecture [15, p 2, Fig. 1]

Number on top of boxes denotes channels, where numbers at bottom of boxes refer to input dimension.

During contracting path (left part) input dimension will be decreased and channels increased. For every step in the contracting path, two 3x3 convolution layers are followed by ReLU and a 2x2 max pooling for down-sampling. Further, at each down-sampling step, input channels are doubled. Multiple contracting steps are combined. After last contracting step, expansive path (right part) starts where input dimension will be increased and input channels will be decreased. For every expansive step, an up-sampling of feature map takes place, followed by a 2x2 convolution, which halves the number of channels. Then, concatenation with the corresponding feature map of contracting path is done (gray arrow in figure 4.2.3), followed by again two 3x3 convolutions and ReLU. Final layer is a 1x1 convolution to map to desired output dimension and single output channel.

4.3 Architecture

Finally, all individual components are introduced and GAT-Denoiser architecture can be defined. First, different neural network layers will be explained and, second, loss and training. As defined in equation 2.6, N is the number of observation and M observation dimension. Therefore, input (noisy sinogram) will be in $\mathbb{R}^{N \times M}$ as well as output (denoised sinogram).

4.3.1 Layers

In figure 4.3.1, detailed GNN architecture can be seen. It is parametrized with *channels*, *heads* and *layers*. The number of channels in convolution can be increased with parameter *channels*. Further, *heads* determine the number of heads used in the GAT layers and parameter *layers* defines how many convolution and GAT layers are stacked together.

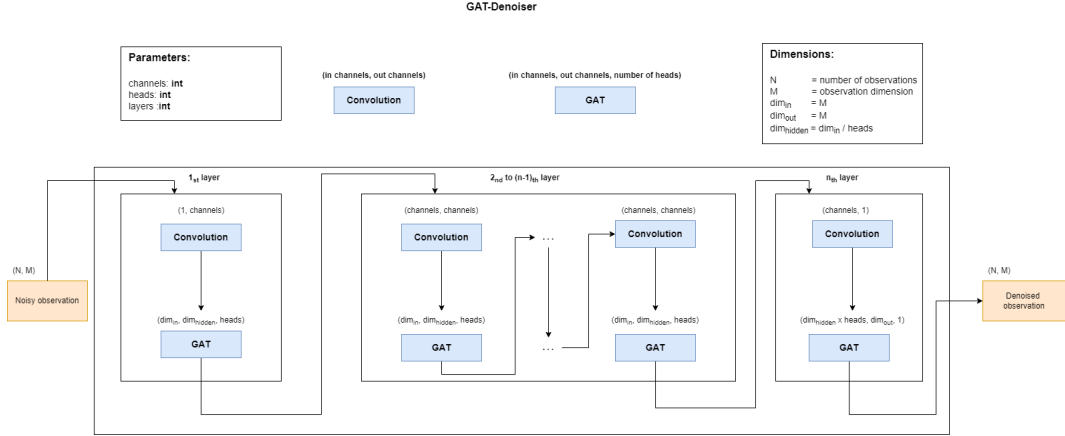


Figure 4.4: Overall GAT-Denoiser architecture

For every layer, first convolution and then GAT is processed. Convolution in the whole network was defined with kernel size of 3 and padding 1, therefore, dimension of convolved signal will not change. Convolution can be defined with different parameters, but output signal needs to have same dimension as input signal. Further, additional convolutional channels can be used for learning. If parameter *channels* > 1, channels are increased in the first convolution layer and decreased in the last one. Parameter *heads* controls multi-head approach for GAT. Input and hidden dimension of GAT is *M* if no heads are used. If multi-head attention is used, hidden dimension will be set to M/heads . In the last GAT layer, everything gets prepared for output dimension and averaging with 1 head is applied.

4.3.2 Training

As already mentioned, an end-to-end learning approach is used where quality of reconstruction is compared in the loss.

Therefore, the outcome of GAT-Denoiser is not directly part of the loss, but first reconstruction will be computed. Reconstructions can be nicely compared with the ℓ_2 -norm:

$$\mathcal{L} = \|x_i - \text{Recon}(\text{GAT-Denoiser}(A(x_i, \theta, s) + \eta))\|_2^2 \quad (4.7)$$

As x_i is part of the loss, access to original object is needed during training.

Further, U-Net will be jointly used with FBP as reconstruction. For that to work, U-Net needs to be first pre-trained with the dataset and learned model can be plugged into GAT-Denoiser. One could also consider training U-Net model jointly, while training GAT-Denoiser.

5

Results

In the current chapter, results of GAT-Denoiser are presented. Further, some interesting findings are illustrated and GAT-Denoiser is compared to U-Net and BM3D[7].

5.1 Dataset

GAT-Denoiser is tested on lodopab-ct dataset [13], which is a benchmark dataset for low-dose ct reconstruction methods and therefore well suited for our domain.

The dataset consists of 35820 train images and 3553 test images. All these images are having resolution 64.

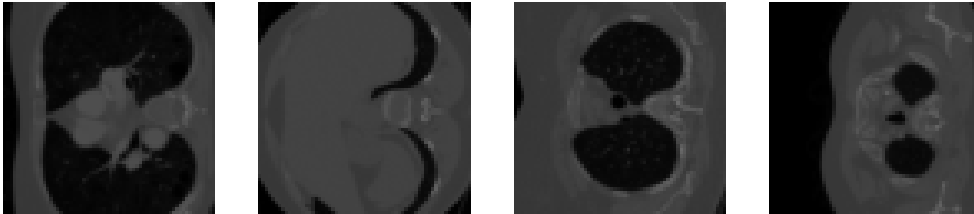


Figure 5.1: Some train images of lodopab-ct dataset.

5.2 Training setup

Training of GAT-Denoiser has been done on the HPC-cluster scicore of the University of Basel. During training, up to 4 titanx GPUs with 12 GB RAM have been used.

5.3 Source code

Source code of the project is available on GitHub³.

³ <https://github.com/cedricmendelin/master-thesis>

5.3.1 Python packages

The following important python packages have been:

5.4 Small Experiments

Some small experiments to find best suited architecture for GAT-Denoiser.

- 1024 train images
- 100 validation images

Test many different settings:

- K-nn size ([2,4,6,8,10,12]) and sampling points / Graph feature dimension (512, 1024, 1536, 2048)
- GAT architecute (Layers, Heads, Loss FBP, Fixed conv)
- Convolution (with, without, multiple channels)
- Loss Sino and FBP
- U-Net with and without
- Different SNR levels
- Learning over SNR range? (slighly not)

5.5 Complete Experiments

Use complete set of experiment dataset.

Compare with :

- Only FBP
- FBP + U-Net
- FBP + Bm3d
- bm3d on sino + FBP
- Eventually same with non-local means

Compare with Bm3d (applied to noisy sinogram, after FBP and after FBP + Unet)

Bibliography

- [1] Tamir Bendory, Alberto Bartesaghi, and Amit Singer. Single-particle cryo-electron microscopy: Mathematical theory, computational challenges, and opportunities. *IEEE signal processing magazine*, 37(2):58–76, 2020.
- [2] David J Brenner and Eric J Hall. Computed tomography—an increasing source of radiation exposure. *New England journal of medicine*, 357(22):2277–2284, 2007.
- [3] Antoni Buades, Bartomeu Coll, and J-M Morel. A non-local algorithm for image denoising. In *2005 IEEE Computer Society Conference on Computer Vision and Pattern Recognition (CVPR'05)*, volume 2, pages 60–65. IEEE, 2005.
- [4] Lawrence Cayton. Algorithms for manifold learning. *Univ. of California at San Diego Tech. Rep*, 12(1-17):1, 2005.
- [5] Rolf Clackdoyle and Michel Defrise. Tomographic reconstruction in the 21st century. *IEEE Signal Processing Magazine*, 27(4):60–80, 2010.
- [6] Ronald R Coifman and Stéphane Lafon. Diffusion maps. *Applied and computational harmonic analysis*, 21(1):5–30, 2006.
- [7] Kostadin Dabov, Alessandro Foi, Vladimir Katkovnik, and Karen Egiazarian. Image denoising by sparse 3-d transform-domain collaborative filtering. *IEEE Transactions on image processing*, 16(8):2080–2095, 2007.
- [8] Allison Doerr. Single-particle cryo-electron microscopy. *Nature methods*, 13(1):23–23, 2016.
- [9] Yifeng Fan and Zhizhen Zhao. Multi-frequency vector diffusion maps. In *International Conference on Machine Learning*, pages 1843–1852. PMLR, 2019.
- [10] Yifeng Fan and Zhizhen Zhao. Cryo-electron microscopy image denoising using multi-frequency vector diffusion maps. In *2021 IEEE International Conference on Image Processing (ICIP)*, pages 3463–3467. IEEE, 2021.
- [11] Marco Gori, Gabriele Monfardini, and Franco Scarselli. A new model for learning in graph domains. In *Proceedings. 2005 IEEE International Joint Conference on Neural Networks, 2005.*, volume 2, pages 729–734. IEEE, 2005.
- [12] Thomas N Kipf and Max Welling. Semi-supervised classification with graph convolutional networks. *arXiv preprint arXiv:1609.02907*, 2016.

- [13] Johannes Leuschner, Maximilian Schmidt, Daniel Otero Baguer, and Peter Maaß. The lodopab-ct dataset: A benchmark dataset for low-dose ct reconstruction methods. *arXiv preprint arXiv:1910.01113*, 2019.
- [14] Johannes Leuschner, Maximilian Schmidt, Poulami Somanya Ganguly, Vladyslav Andriashen, Sophia Bethany Coban, Alexander Denker, Dominik Bauer, Amir Hadjifaradji, Kees Joost Batenburg, Peter Maass, et al. Quantitative comparison of deep learning-based image reconstruction methods for low-dose and sparse-angle ct applications. *Journal of Imaging*, 7(3):44, 2021.
- [15] Olaf Ronneberger, Philipp Fischer, and Thomas Brox. U-net: Convolutional networks for biomedical image segmentation. In *International Conference on Medical image computing and computer-assisted intervention*, pages 234–241. Springer, 2015.
- [16] Amit Singer. Mathematics for cryo-electron microscopy. In *Proceedings of the International Congress of Mathematicians: Rio de Janeiro 2018*, pages 3995–4014. World Scientific, 2018.
- [17] Amit Singer and H-T Wu. Vector diffusion maps and the connection laplacian. *Communications on pure and applied mathematics*, 65(8):1067–1144, 2012.
- [18] Daniel Spielman. Spectral graph theory. *Combinatorial scientific computing*, 18, 2012.
- [19] Peter Toft. The radon transform. *Theory and Implementation (Ph. D. Dissertation)(Copenhagen: Technical University of Denmark)*, 1996.
- [20] Ashish Vaswani, Noam Shazeer, Niki Parmar, Jakob Uszkoreit, Llion Jones, Aidan N Gomez, Łukasz Kaiser, and Illia Polosukhin. Attention is all you need. *Advances in neural information processing systems*, 30, 2017.
- [21] Petar Veličković, Guillem Cucurull, Arantxa Casanova, Adriana Romero, Pietro Lio, and Yoshua Bengio. Graph attention networks. *arXiv preprint arXiv:1710.10903*, 2017.
- [22] Ulrike Von Luxburg. A tutorial on spectral clustering. *Statistics and computing*, 17(4): 395–416, 2007.
- [23] Yue Wang, Yongbin Sun, Ziwei Liu, Sanjay E Sarma, Michael M Bronstein, and Justin M Solomon. Dynamic graph cnn for learning on point clouds. *Acm Transactions On Graphics (tog)*, 38(5):1–12, 2019.
- [24] Felix Wu, Amauri Souza, Tianyi Zhang, Christopher Fifty, Tao Yu, and Kilian Weinberger. Simplifying graph convolutional networks. In *International conference on machine learning*, pages 6861–6871. PMLR, 2019.



Mathematical tools

A.1 signal-to-noise-ratio (SNR)

TODO:

A.2 3D rotation matrix

A rotation matrix is a transformation matrix used to perform rotations. In 3D case, matrix for rotating one single axis can be described as:

$$R_{e_x}(\theta) \begin{bmatrix} 1 & 0 & 0 \\ 0 & \cos \theta & -\sin \theta \\ 0 & \sin \theta & \cos \theta \end{bmatrix} \quad (\text{A.1})$$

$$R_{e_y}(\theta) \begin{bmatrix} \cos \theta & 0 & \sin \theta \\ 0 & 1 & 0 \\ -\sin \theta & 0 & \cos \theta \end{bmatrix} \quad (\text{A.2})$$

$$R_{e_z}(\theta) \begin{bmatrix} \cos \theta & -\sin \theta & 0 \\ \sin \theta & \cos \theta & 0 \\ 0 & 0 & 1 \end{bmatrix} \quad (\text{A.3})$$

where e_x, e_y, e_z corresponds to the axis unit-vector (for x: $(1, 0, 0)$, etc.) and $\theta \in \mathbb{R}$. To combine the single axis rotations, matrices can be multiplied with each other:

$$R(\theta) = R_{e_x}(\theta)R_{e_y}(\theta)R_{e_z}(\theta) \quad (\text{A.4})$$

In equation A.4, angle θ is the same for all axis, which does not have to be.

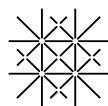
A.3 Power Iterations

Power iteration, also called power method, is an iterative method that approximates largest eigenvalue of a diagonalizable matrix A .

The algorithm starts with a random vector b_0 or an approximation of the dominant eigenvector.

$$b_{k+1} = \frac{Ab_k}{\|Ab_k\|} \quad (\text{A.5})$$

It will not necessarily converges. The algorithm will converge if A has an eigenvalue strictly grater than its other eigenvalues and initial vector b_0 is not orthogonal to the eigenvector associated with the largest eigenvalue.



Declaration on Scientific Integrity

(including a Declaration on Plagiarism and Fraud)

Translation from German original

Title of Thesis: _____

Name Assesor: _____

Name Student: _____

Matriculation No.: _____

With my signature I declare that this submission is my own work and that I have fully acknowledged the assistance received in completing this work and that it contains no material that has not been formally acknowledged. I have mentioned all source materials used and have cited these in accordance with recognised scientific rules.

Place, Date: _____ Student: _____

Will this work be published?

☐ No

☐ Yes. With my signature I confirm that I agree to a publication of the work (print/digital) in the library, on the research database of the University of Basel and/or on the document server of the department. Likewise, I agree to the bibliographic reference in the catalog SLSP (Swiss Library Service Platform). (cross out as applicable)

Publication as of: _____

Place, Date: _____ Student: _____

Place, Date: _____ Assessor: _____

Please enclose a completed and signed copy of this declaration in your Bachelor's or Master's thesis .